J Mater Sci: Mater Electron (2023) 34:560

Analysis of opto-electrical properties of Cu/Sr–W/n-Si (MIS) Schottky barrier diode for optoelectronic applications

V. Balasubramani[1,*], R. Marnadu[2], R. Priya[3], S. Thanikaikarasan[1], A. Sivakumar[4], Mohd. Shkir[5,6], F. Maiz[5,7], Woo Kyoung Kim[8], and Vasudeva Reddy Minnam Reddy[8,*]

[1] *Department of Physics, Saveetha School of Engineering, Saveetha Institute of Medical and Technical Sciences, Chennai 602 105, Tamil Nadu, India*
[2] *Department of Physics, Govt Arts And Science College, Sivakasi, 626124, , Tamil Nadu , India*
[3] *Department of Physics, Adhiyamaan College of Engineering, Hosur, Tamilnadu 635109, India*
[4] *Key Laboratory of High-temperature and High-pressure Study of the Earth's Interior, Institute of Geochemistry, Chinese Academy of Sciences, , Guiyang, Guiyang 550081, China*
[5] *Department of Physics, Faculty of Science, King Khalid University, P.O. Box 9004, Abha 61413, Saudi Arabia*
[6] *Division of Research and Development, Lovely Professional University, Phagwara, Punjab 144411, India*
[7] *Laboratory of Thermal Processes, Center for Energy Research and Technology, BP: 95, Borj-Cedria, Tunisia*
[8] *School of Chemical Engineering, Yeungnam University, Gyeongsan 38541, Republic of Korea*

Received: 21 October 2022
Accepted: 20 December 2022
Published online: 16 February 2023

ABSTRACT

In this study, the Schottky diodes based on an interfacial layer of Sr–W thin film were fabricated. Thin films were coated on glass and silicon substrates by low-cost jet nebulizer spray pyrolysis (JNSP) coating technique with optimized substrate temperatures 500 °C. Structural, surface morphology, optical, and electrical characteristics of Sr–W thin film were investigated. In particular, the *I–V* characteristics of Cu/Sr–W/n-Si diodes in dark and light excitations were analysed. The maximum barrier height (Φb) for the diode fabricated 6 wt% tungsten under xenon lamp light irradiation was observed at 0.83 eV. Also, near ideal ideality factor (n) of the diode parameters, it was found at highest 6 wt% tungsten. The results show that diodes are more appropriate for the improvement of good quality photodiodes as well as photodetector applications.

Address correspondence to E-mail: balasubaramaniv3@gmail.com; drmvasudr9@gmail.com

https://doi.org/10.1007/s10854-022-09733-1

1 Introduction

A metal–semiconductor (MS) Schottky barrier diode is formed by direct contact between the metal and semiconductor in the conventional Schottky contact. Schottky diodes are frequently employed in RF and microwave applications such as varactors, detectors, mixers, multipliers, low-voltage reference circuits, and optoelectronic devices [1–5]. Schottky diodes have several advantages, which includes high operation frequency, quick switching speed, and minimal forward voltage loss.

Besides other diodes, the metal–insulator–semiconductor (MIS) diode is best for analysing semiconductor surfaces when the insulator layer is thin (< 60A). Quantum mechanical tunnelling mechanism allows current to transfer between metal and semiconductor by this condition. Barrier height (BH) of metal–insulator–semiconductor (MIS) connections is an essential factor that governs their electrical properties [6–8].

Consequently, the insulating layer is vital in controlling the electrical properties of MIS diodes. Furthermore, an increase in the annealing temperature and doping concentration, the parameters like barrier width, ideality factor, and resistivity can be managed [9]. Fermi level depinning caused due to charge neutrality level reflects the barrier height reduction, low-resistance quasi-Ohmic contacts for optoelectronic devices [10]. MIS Schottky barrier has been the subject of numerous investigations, owing to the benefits it provides, such as lower leakage current and higher rectification ratio especially wide bandgap semiconductor used in the photodetector [11]. The work function of the metal contact, insulator thickness, qualities of surface states at the insulator–semiconductor (IS) interface, device temperature, and the semiconductor dopant type are all.

Currently, researchers are focussing on preventing the Fermi pinning effect in Schottky barrier diodes (SBDs) by using metal-oxide thin films with various dopants as insulating layers. Accordingly, the metal-oxide sheath on the insulating layer lowers the contact resistance. Strontium possess high optical transmittance, wide bandgap (> 3.61 eV) due to its high optical transmittance, and electrical conductivity [12]. It was observed that at maximum substrate temperature (500 °C), Barrier height gradually increases both dark and light conditions [13]. Fan et al., reported that a variety of characterization techniques had been used to explore the production and properties of Sr thin films annealed at different temperatures. According to their electrical analysis, elevating the annealing temperature/doping concentration enhanced the insulating properties of Sr thin films. Strontiumm thin film is activated by post-annealing at different temperatures and doping concentrations, resulting in a low-leakage current density (10^{-8} Acm^{-2} at 3 V) and aerial capacitance of more than 350nF cm^{-2} at 20 Hz [14].

There are numerous synthesis techniques available for the formation of thin film. However, jet nebulizer spray pyrolysis (JNSP) offers a distinct advantage due to its low-cost, non-vacuum approach for a wide range of applications that can create a high-quality film from a small amount of precursor [15].

In this study, fabrication of Metal–insulator–semiconductor (MIS)-structured Schottky diodes are performed and evaluated in dark and light condition with tungsten trioxide as dopant material. The diode characteristics are enhanced to examine the different dopant percentages. The *I–V* characteristics, particularly diode parameters saturation current (I_o), ideality factor (n,), and barrier height (ϕ_B) are calculated and discussed in detail below.

2 Experimental techniques

2.1 Methods for thin-film preparation

All chemicals required for the preparation of Sr–W thin film were purchased from Sigma-Aldrich with > 98% of purity. The host precursor solution is prepared by weighing 0.31706 g of Strontium chloride and dissolved in 10 ml of Ethanol, stirred for about half an hour. Various dopant concentrations of tungsten chloride (W) (2%, 4%, and 6 wt%) were added separately to the host precursor solution. Homogeneous mixture for each concentration is obtained by stirring the solutions thoroughly and kept undisturbed for 2 h. The glass substrate was cleaned in an ultrasonic bath with acetone, ethanol, and deionized water in order to prepare them for deposition. By JNSP technique, Sr–W thin film was coated on the glass substrate at an optimized temperature of 500 °C.

2.2 Process of n silicon wafer cleaning

Lowering of defect density and high yield was obtained by cleaning of n silica wafer. The native oxide layer on the n-type Si substrate was removed after 15 min of immersion in piranha solution ($3H_2SO_4$:$1H_2O_2$) and 1% HF solution.

2.3 Cu/Sr–W/n-Si-type Schottky diode fabrication

The prepared solution of Sr–W was sprayed on the 1 cm x 1 cm n-type silica wafer by the JNSP technique. Schottky's contact of copper (Cu) coated on a surface of Sr–W layer in thickness of metal contact is 500 mm and diameter 4 mm. via DC sputtering using high-clarity Cu target. The ohmic contact Ag paste is placed at both ends. Figure 1 shows the structure of Cu/Sr–W/n-Si MIS-type Schottky diode, where it is observed that both the leads are connected to Keithley 6517-B electrometer.

2.4 Characterization techniques

The coated film was subjected to different characterization techniques. Stylus Profilometer detector (model: SJ-30) was used to measure the thickness of the film. The structural parameters and phase identification were performed with an Ultima III Rigaku X-ray diffractometer at a scanning rate of 0.21 min^{-1} in the range of 20–80 with Cukα radiation (wavelength = 1.5406 Å). Surface morphology of the coated films was analysed by scanning electron microscopy and chemical composition (EDX) methods. The prepared thin film features were ventilated using the scanning electron microscopy (JEOL-JSM-IT-200) of magnification up to ×3,00,000. Optical studies were carried out by UV–Visible spectrophotometer (JASCO UV–Vis V-770PC) in the wavelength range of 190–1100 nm. Electrical properties of Ag/SrO–W/n-Si/Ag junction diodes were measured using Keithley source meter 6517-B.

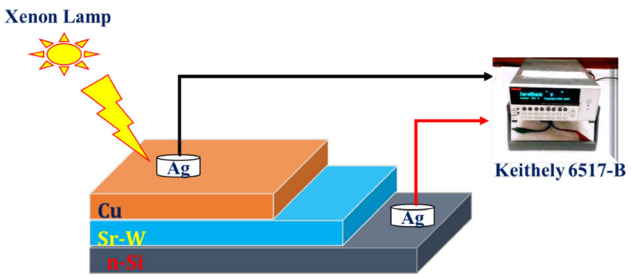

Fig. 1 Schematic diagram of Cu/Sr–W/n-Si Schottky diode

3 Results and discussion

3.1 Thickness measurement

Film thickness produced by spray pyrolysis is greatly influenced by concentration of the solutions, treatment of the substrates, and management of the spray duration. Figure 2 depicts the thickness of the Sr–W films. It specifies the thickness of the film for pure Sr and dopant weight percentages from 2, 4, and 6 wt% as 357, 413, 453, and 475 nm. The film thickness gets raised when the doping concentration is increased. This is due to the porous structure of the film produced when the doping concentration remains low. More doping atoms fill the defects as the doping concentration rises, and new layers of crystallite orientation are created, increasing the film thickness [16]. This elevated thickness may influence the colour variation. Therefore, the colour of the film finally changes into pastel yellow.

3.2 XRD structural analysis

X-ray diffraction patterns (XRD) of pure and Sr–W at different concentrations of 2, 4, and 6 wt% are shown in Fig. 3. Strontium films with W dopant were deposited at 500 °C annealing temperature. It is observed that the diffraction position at $2\theta^\circ$ = 13.10, 22.58, 31.93, and 39.41 indexes as (111), (220), (400), and (422) which confirms the JCPDS Card 01-0886.

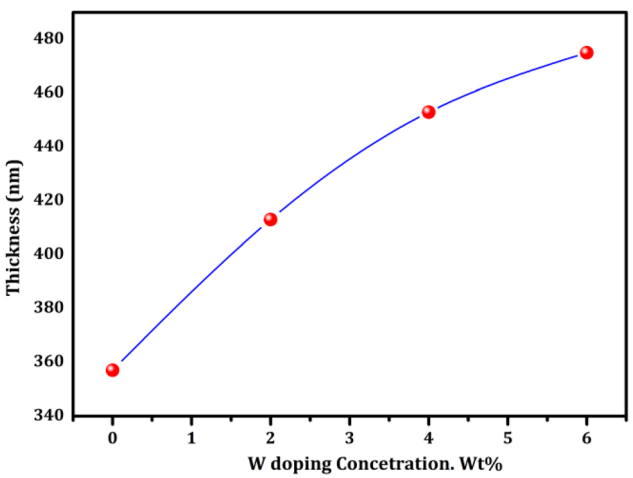

Fig. 2 Thickness of Sr–W films

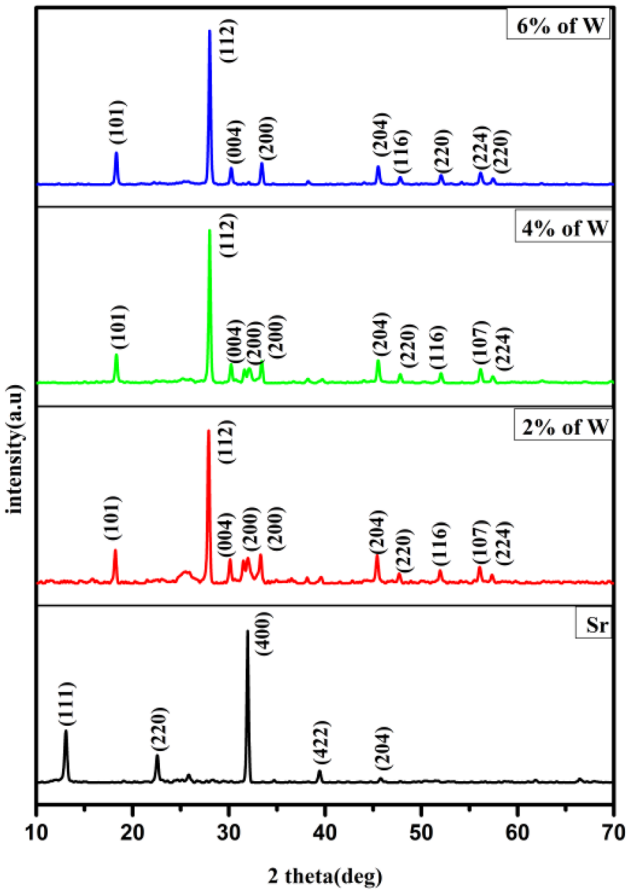

Fig. 3 X-ray diffraction pattern of Sr–W films

Different concentrations of W high-intensity peak positions at 28.00 attributed to (112) and small peaks at 18.35, 45.48, 56.16 attributed to (101), (204), (220) indicating that the tetragonal structure is proved from JCPDS card 89-2568. This specifies that pure Sr film has cubic structure and the presence of dopant concentrations has influenced a phase change into tetragonal. This change confirms the successful incorporation of the W–Sr lattice site and might be owing to lesser W ionic radius of 210 pm compared to that of Sr 255 pm that may be influenced by the crystalline parameters of the Sr host lattice [17, 18].

The average crystallite size and other structural parameters can be calculated from the Scherrer formula by the following relation [19]:

$$D = \frac{0.89\lambda}{\beta \operatorname{Cos}\theta} \tag{1}$$

$$\varepsilon = \frac{\beta \operatorname{Cos}\theta}{4} \tag{2}$$

$$\delta = \frac{1}{D^2} \tag{3}$$

$$\mathrm{SF} = \left[\frac{2\pi^2}{4(3\tan\theta)^{\frac{1}{2}}}\right]\beta. \tag{4}$$

The calculated structural parameters of films are listed in Table 1. The average crystallite size of W are 47.42, 48.67, 50.08, and 54.0 nm for the films with pure SrO, (2, 4, and 6 wt%) W dopants, respectively.

The calculated crystallite size is increased with doping concentration. Increase in crystallite might be due to the influence of W dopant on Sr lattice. Calculated dislocation density value of film decreases with increasing W doping concentrations. This indicates that improved crystallinity and prepared films are found to be good in quality. The sample prepared with W at 6 wt% film shows a minimum average value of micro strain. Due to the removal of defects in the lattice with increase in W doping concentration, rendered photodiode properties of MIS structure diodes.

3.3 UV spectroscopy studies

The absorbance spectra for all coated films with wavelengths in the visible range of 200 to 800 nm are shown in Fig. 4. As the concentration of dopant rises, the absorbance of Sr–W gradually increased. Additionally, the dopant films displayed improved UV–visible absorption with an increase in W concentration (0–6 wt%), which is due to variations in the bandgap's localized state density brought by increasing W concentrations changing the unsaturated bond density. On comparison to pure Sr thin films, 6 wt% weight percent Sr–W films have the highest absorbance, making them the most suitable for photodiode application [20].

According to the Tauc's plot relation, optical bandgap (E_g) values can be calculated [21] using the following relation:

$$(\alpha h\upsilon) = A\left(h\upsilon - E_g\right)^n, \tag{5}$$

where n is taken 1/2 since the film is a direct bandgap material, A is a constant, and Planck's constant is h. Figure 5 shows the intercept results bandgap that gets lowered with increasing dopant concentration. The corresponding bandgap values are listed in Table 2, which notifies that decreasing bandgap values and E_g value of 3.68 eV have a greater surface-to-

Table 1 Structural parameters of the Sr–W thin films

Sample code	Diffraction 2 (θ) (°)	Inter planar distance (d) (Å)	FWHM (radians)	Crystallite size (D) nm	Dislocation density (δ) (10^{14} lines m^{-2})	Micro strain (ε)
SrO	13.10	6.7583	0.00145	95.72	1.0912	0.000362
	22.58	3.9374	0.00233	60.59	2.7236	0.000572
	31.93	2.8021	0.00116	12.36	6.5446	0.000280
	39.41	2.2859	0.00700	21.03	2.2602	0.001649
2 wt% of W	18.21	4.8713	0.00350	40.11	6.2128	0.000864
	27.88	3.1991	0.00262	54.39	3.3797	0.000637
	45.39	1.9980	0.00233	64.40	2.4105	0.000538
	56.08	1.6399	0.00700	22.43	1.9866	0.001540
4 wt% of W	18.34	4.8355	0.00204	68.77	2.1142	0.000504
	27.99	3.1867	0.00175	81.61	1.5013	0.000425
	45.48	1.9942	0.00350	42.95	5.42023	0.000807
	56.11	1.6389	0.00291	53.85	3.4483	0.000644
6 wt% of W	18.35	4.8344	0.00233	60.19	2.7601	0.000576
	28.00	3.1860	0.00233	61.24	2.6664	0.000566
	45.48	1.9943	0.00233	64.42	2.4090	0.000538
	56.16	1.6377	0.00350	44.89	4.9604	0.000772

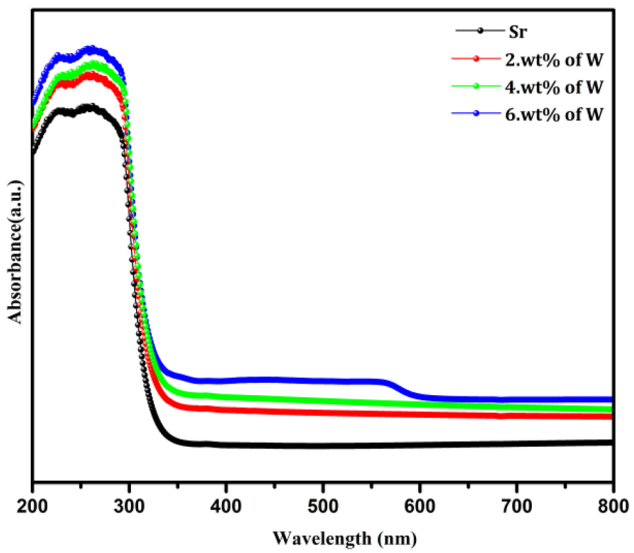

Fig. 4 Absorption spectra of Sr–W films

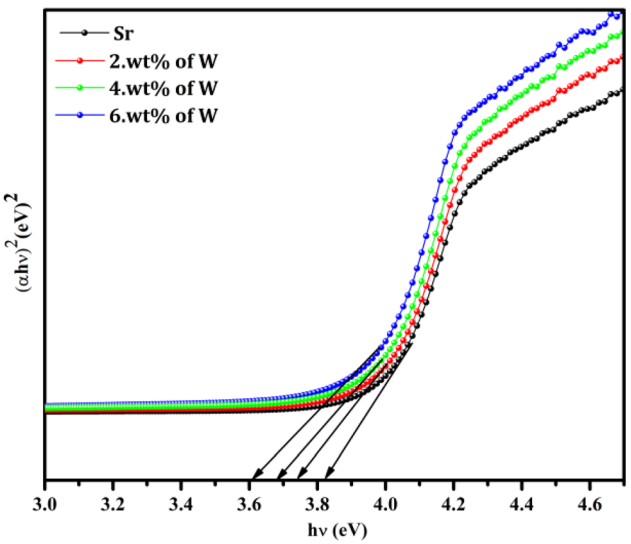

Fig. 5 Tauc's plot of Sr–W films

volume ratio, which helps in improving light absorption for better MIS-based diode performance [22].

3.4 AFM analysis

Sr–W films AFM 3D and topography view of the thin film scanned at 10 µm × 10 µm areas are given in Fig. 6. AFM images are employed to characterize the surface morphology information of the coated films

Table 2 Bandgap energy value Sr–W thin films

Sample code	Bandgap (E_g) (eV)
SrO	3.81
2 wt% of W	3.73
4 wt% of W	3.68
6 wt% of W	3.61

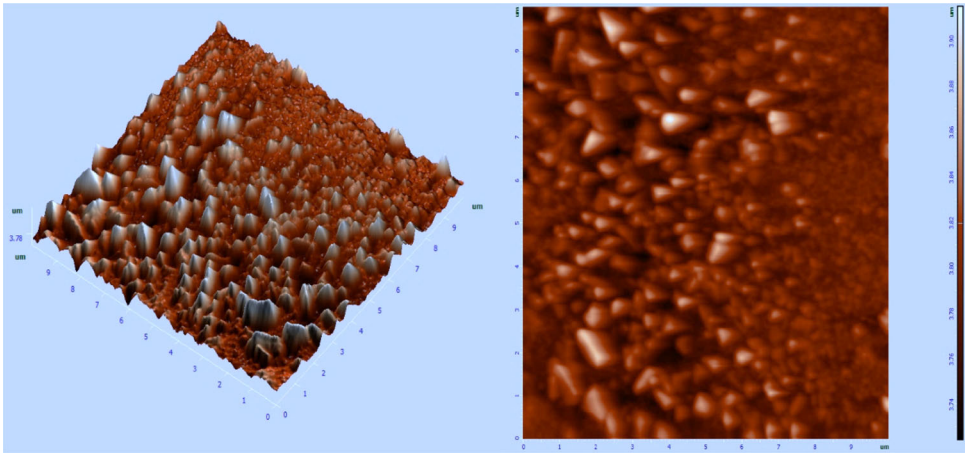

Fig. 6 AFM 3D and topography view of Sr–W films

in order to investigate the surface roughness and nature of the grains.

The following relation can be used to compute the roughness's root square (RMS) [23]:

$$\mathrm{RMS} = \sqrt{\frac{1}{N}\sum_{i=1}^{N} Z_i^2}. \tag{6}$$

The calculated root mean square is 22.35 nm and average roughness, 16.74 nm. The film's surface is covered with sharp needle and rod-like features that are organized more densely in the topographical view. Smooth surface hillock's structure and formation of an unbroken layer of Sr–W on the n-Si surface are confirmed by AFM pictures. These effects can strengthen the rectifying capabilities of Schottky diodes and MIS structures.

4 Electrical property

4.1 DC electrical property

Figure 7 shows the electrical conductivity of Sr–W films measured at temperature range of 30 °C to 120 °C. Table 3 shows the electrical parameters like resistivity (Ω cm), conductivity (S/cm), and activation energy (eV) of Sr with W for different concentrations calculated using the following relation [24]:

$$\sigma_{\mathrm{dc}} = \left(\frac{d}{A}\right)\left(\frac{I}{V}\right) \mathrm{S/cm}. \tag{7}$$

The substrate temperature (500 ° C) may influence grain boundaries and the crystal lattice deficit of the films gets reduced [25]. The electrical conductivity for pure Sr is 1.605×10^{-10} (S/cm) and dopant has rapidly increased from 4.472×10^{-11} (S/cm) to 1.427×10^{-9} (S/cm). The barrier height and activation energy plots, however, are unaffected by this bias dependence. The significant resistance results in non-linearity in the *I–V* characteristics of the Schottky diode when there are barrier inhomogeneities that cause a large number of parallel, non-interacting diodes to act at once [26–28].

The Sr–W films Arrhenius plot is depicted in Fig. 8. The activation energy can be calculated by using the Arrhenius plot to generate the following equation [29]:

$$\text{Actiation energy } (E_a) = \text{slope value} \times \left(\frac{K_B}{e}\right)(\mathrm{eV}) \tag{8}$$

The activation energy decreases as the substrate temperature rises. The E_a value and resistivity decreased, as is shown in Table 3. E_a decreased from 0.3417 to 0.0771 while the proportion of dopant concentration raised. As a result, the conductivity of the system improves. Consequently, in photodiode applications, this feature promotes good diode performance [30].

4.2 Cu/Sr–W/n-Si diode fabrication evaluation

The forward and reverse bias measurement *I–V* plot of Cu/Sr–W/n-Si MIS diode was measured from − 2 to + 2 V under both dark and light conditions Fig. 9. The thermionic emission occurs when the thermal energy provided to charge carriers exceeds the binding potential, allowing electrons to escape from

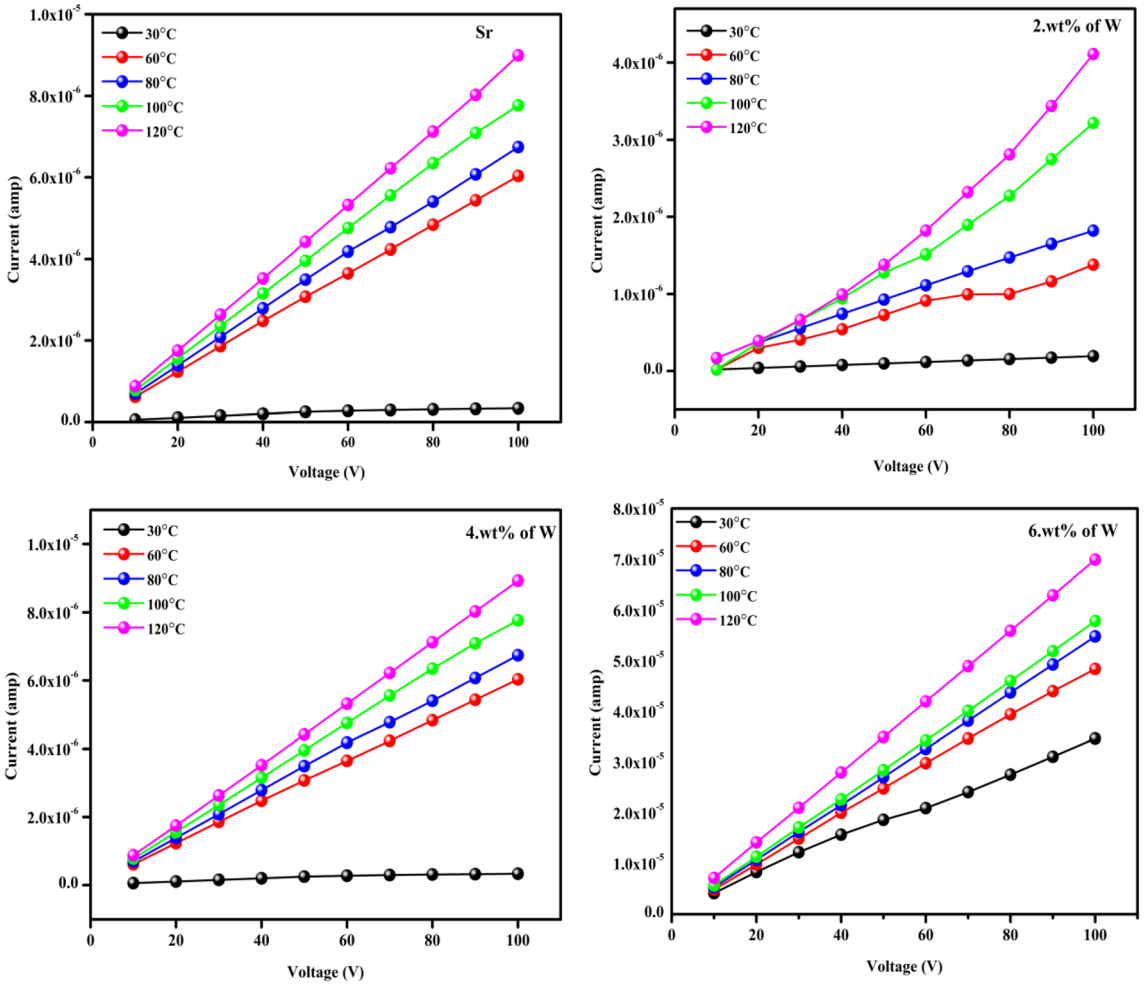

Fig. 7 Current vs voltage plot of Sr–W films

Table 3 Electrical parameters for Sr–W thin films

Sample code	Resistivity $\times 10^{10}$ (Ω cm)	Conductivity (S/cm)	Activation energy (eV)
SrO	2.1048	1.605×10^{-10}	0.3417
2 wt% of W	6.4370	4.472×10^{-11}	0.2223
4 wt% of W	2.1044	1.607×10^{-10}	0.2822
6 wt% of W	3.5490	1.427×10^{-9}	0.0771

the solid's surface. Electrons or ions can be used as charge carriers [31–37].

The following relationship is utilized to analyse the current transmission mechanism of the Cu/Sr–W/n-Si diodes based on the thermionic emission theory. According to the thermionic emission theory, the current–voltage characteristics are given by [38]

$$J = J_s\left[\exp\left(\frac{qV}{nk_BT}\right) - 1\right], \tag{9}$$

where J_o is the saturation current density, q is the electron charge, V is the voltage, n is the ideality factor of the fabricated diode, k_B is the Boltzmann constant, and T is the absolute temperature..

Richardson–Dushman equation, which is [39]

$$J_s = \frac{I_S}{A} = A^*T^2\exp\left[\frac{-q\phi_B}{k_BT}\right], \tag{10}$$

where J is emission density in amperes/cm^2, A is the area of Schottky contact, and A^* is the effective area

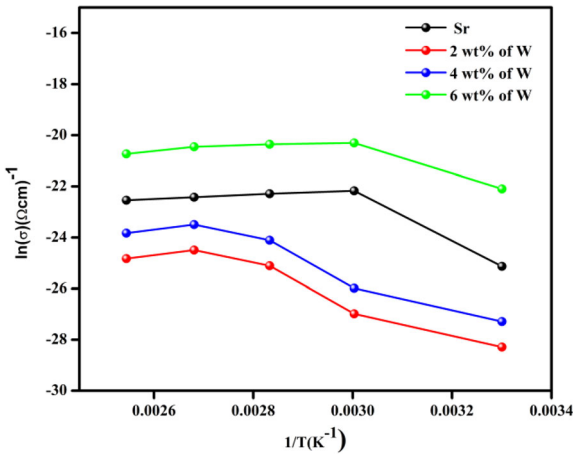

Fig. 8 Arrhenius plot of Sr–W films

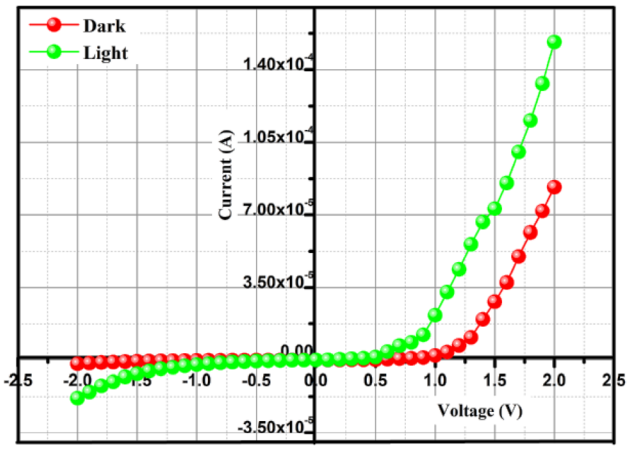

Fig. 9 *I–V* plot of Cu/Sr–W/n-Si Schottky diode

of Richardson constant 120 A cm^{-2} K^{-2}. ϕ_B is the effective barrier height, T is temperature in kelvins (K), and k, the Boltzmann constant, is 8.6164×10^{-5} eV K^{-1}. The work function's emission density is an exponential function [40–46].

The other diode parameters such as ideality factor (n) and barrier height (ϕ_B) were calculated by following relations [47, 48]:

$$n = \frac{q}{k_B T}\left(\frac{dV}{d(\ln J)}\right) \tag{11}$$

$$\Phi_B = k \cdot T/q \ \ln(AA \times T_2/I_o) \tag{12}$$

Figure 10 shows of semi-logarithmic ln(J)–V curve Cu/Sr–W/n-Si Schottky diode and calculated values ideality factor barrier height and saturation current. This study indicates that the W dopant's impact causes a decrease in n and an increase in barrier height, which is utilized as an interfacial layer and

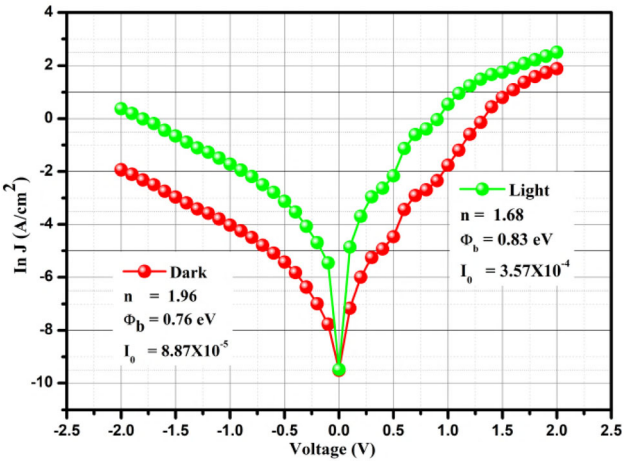

Fig. 10 Semilogarithmic plot of Cu/Sr–W/n-Si Schottky diode

also noticed that the barrier height rises with W concentration, which might be caused by the valence band's shrinkage. Furthermore, the computed n value is bigger than the unity. The n value must be equal to unity for an ideal Schottky diode with current dominated by thermionic emission. The reported high values of n can be attributed to the Rs, non-homogeneous barrier, tunnelling-current, interlayer presence, and Nss [49–51]. the calculated values are minimum n values 1.68 factor barrier height 0.83 eV and saturation current 3.57×10^{-4} are observed in light condition. The presence of interface states between the Sr–W film and n-Si and the high value of ideality factor greater than unity ($n > 1$) are attributable to voltage drop across the temperature and are minimized in the film at 500 °C. The inhomogeneities of barrier height and interface states are dependent on the substrate temperature and are minimized in the film at 500 °C, resulting in a diode with a high ideality factor [52–54]. The oxygen defect states are reduced when the annealing process is carried out at a higher temperature, and therefore the barrier height is reduced[55, 62, 63].

5 Conclusion

Cu/Sr–W/n-Si-structured Schottky diodes were successfully fabricated with various concentrations of W using JNSP method. The film thickness then rises when the addition of doping concentration is increased. The existence of dual phase cubic and tetragonal structure is confirmed by XRD pattern with predominant orientations along (1 1 2)

directions. The minimum bandgap 3.61 eV energy is obtained at higher doping concentration compared with the other films. AFM images confirm the smooth surface and growth of an unbroken layer of the Sr–W on n-Si surface. *I–V* nature of Cu/SrW/n-Si-type MIS diode indicates higher rectifying activity with minimum n values of 1.68. The results consummated that the device, MIS-structured diode with light condition films signify inconsistent photodiode performance associated with other devices.

Acknowledgements

The authors extend their appreciation to the Research Center for Advanced Materials Science (RCAMS), King Khalid University, Saudi Arabia, for funding this work under grant number RCAMS/KKU/020-22.

Author contributions

All the authors contributed to the study conception and design. Materials preparation, data collection, and analysis were performed by VB, RM, ST, RP, AS, MS and FM, WKK, and VRMR. All authors read and approved the final manuscript. VB: writing—original draft, methodology, conceptualization, visualization, methodology, supervision, writing—review and editing. RM: conceptualization, visualization, writing—review and editing. ST: writing—review and editing. RP: writing—review and editing. AS: writing—review and editing. MS and FM: writing—review and editing, funding acquisition. WKK; writing—review and editing VRMR; writing—review and editing and Supervision.

Data availability

Data will be made available on reasonable request.

Declarations

Conflict of interest There are no conflict of interests and, if accepted, the article will not be published elsewhere in the same form, in any language without the written consent of the publisher.

References

1. X. Yang, Y. Gu, M.A. Migliorato, Y. Zhang, Impact of insulator layer thickness on the performance of metal–MgO–ZnO tunneling diodes. Nano Res. **9**(5), 1290–1299 (2016)
2. M. Raja, J. Chandrasekaran, M. Balaji, B. Janarthanan, Impact of annealing treatment on structural and dc electrical properties of spin coated tungsten trioxide thin films for Si/WO3/Ag junction diode. Mater. Sci. Semicond. Process. **56**, 145–154 (2016)
3. N. Okada, N. Uchida, T. Kanayama, Fermi-level depinning and contact resistance reduction in metal/n-Ge junctions by insertion of W-encapsulating Si cluster films. Appl. Phys. Lett. **104**(6), 062105 (2014)
4. C.H. Lin, C.W. Liu, Metal-insulator-semiconductor photodetectors. Sensors **10**(10), 8797–8826 (2010)
5. V. Balasubramani, P.V. Pham, A. Ibrahim, J. Hakami, M.Z. Ansari, T.K. Le, Enhanced photosensitive of Schottky diodes using SrO interfaced layer in MIS structure for optoelectronic applications. Opt. Mater. **129**, 112449 (2022)
6. C. Fan, A. Liu, Y. Meng, Z. Guo, G. Liu, F. Shan, Solution-processed SrO x-gated oxide thin-film transistors and inverters. IEEE Trans. Electron. Devices **64**(10), 4137–4143 (2017)
7. M. Thirumoorthi, J. Thomas Joseph Prakash, Structure, optical and electrical properties of indium tin oxide ultra-thin films prepared by jet nebulizer spray pyrolysis technique. J. Asian Ceram. Soc. **4**(1), 124–132 (2016)
8. F.Z. Pür, A.D.E.M. Tataroğlu, Analysis of the series resistance and interface states of Au/Si_3N_4/n-Si (metal–insulator–semiconductor) Schottky diodes using I-V characteristics in a wide temperature range. Phys. Scr. **86**(3), 035802 (2012)
9. S. Bhuvaneswari, M. Seetha, J. Chandrasekaran, R. Marnadu, Y. Masuda, O.M. Aldossary, M. Ubaidullah, Fabrication and characterization of p-Si/n-In_2O_3 and p-Si/n-ITO junction diodes for optoelectronic device applications. Surf. Interfaces **23**, 100992 (2021)
10. R. Marnadu, J. Chandrasekaran, S. Maruthamuthu, V. Balasubramani, P. Vivek, R. Suresh, Ultra-high photoresponse with superiorly sensitive metal-insulator-semiconductor (MIS) structured diodes for UV photodetector application. Appl. Surf. Sci. **480**, 308–322 (2019)
11. K. Sasikumar, R. Bharathikannan, M. Raja, Effect of annealing temperature on structural and electrical properties of Al/ZrO_2/p-Si MIS Schottky diodes. SILICON **11**(1), 137–143 (2019)
12. S. Chand, J. Kumar, Origin of Non-ideal Current-Voltage Characteristics of Metal-Semiconductor Contact: A Numerical Study (2000)
13. V. Balasubramani, J. Chandrasekaran, R. Marnadu, P. Vivek, S. Maruthamuthu, S. Rajesh, Impact of annealing temperature

on spin coated V_2O_5 thin films as interfacial layer in cu/V_2O_5/n-si structured schottky barrier diodes. J. Inorg. Organomet. Polym. Mater. **29**(5), 1533–1547 (2019)

14. V. Balasubramani, J. Chandrasekaran, T.D. Nguyen, S. Maruthamuthu, R. Marnadu, P. Vivek, S. Sugarthi, Colossal photosensitive boost in Schottky diode behaviour with Ce-V_2O_5 interfaced layer of MIS structure. Sens. Actuators A **315**, 112333 (2020)
15. V. Balasubramani, J. Chandrasekaran, V. Manikandan, R. Marnadu, P. Vivek, P. Balraju, Influence of rare earth doping concentrations on the properties of spin coated V_2O_5 thin films and Cu/Nd-V_2O_5/n-Si Schottky barrier diodes. Inorg. Chem. Commun. **119**, 108072 (2020)
16. V. Balasubramani, J. Chandrasekaran, V. Manikandan, T.K. Le, R. Marnadu, and P. Vivek. "Upgraded photosensitivity under the influence of Yb doped on V_2O_5 thin films as an interfacial layer in MIS type Schottky barrier diode as photodiode application." *Journal of Solid-State Chemistry* (2021): 122289.
17. V. Balasubramani, J. Chandrasekaran, V. Manikandan, T.K. Le, R. Marnadu, P. Vivek, Improved photodetector performance of high-k dielectric material (La) doped V_2O_5 thin films as an interfacial layer in Schottky barrier diodes. Surf. Interfaces **25**, 101297 (2021)
18. H.A. Mohamed, p-Type transparent conducting copper-strontium oxide thin films for optoelectronic devices. Eur. Phys. J. Appl. Phys. **56**, 30301 (2011)
19. U. Chaitra, A.M. Ali, M.G. Mahesha, A. Kompa, D. Kekuda, K.M. Rao, Property evaluation of spin coated Al doped ZnO thin films and Au/AZO/FTO Schottky diodes. Superlattices Microstruct. **155**, 106903 (2021)
20. B. Roy, J.D. Perkins, T. Kaydanova, D.L. Young, M. Taylor, A. Miedaner, C. Curtis, H.-J. Kleebe, D.W. Readey, D.S. Ginley, Preparation and characterization of sol–gel derived copper–strontium–oxide thin films. Thin Solid Films **516**, 4093–4101 (2008)
21. D. Louloudakis, M. Varda, E.L. Papadopoulou, M. Kayambaki, K. Tsagaraki, V. Kambilafka, M. Modreanu, G. Huyberechts, E. Aperathitis, Properties of strontium copper oxide (SCO) deposited by PLD using the 308 nm laser and formation of SCO/Si heterostructures. Phys. Status Solidi A **207**, 1726–1730 (2010)
22. H.A. Mohamed, p-Type transparent conducting copper-strontium oxide thin films for optoelectronic devices. Eur. Phys. J. Appl. Phys. **56**, 30301 (2011)
23. P. Balasubramanian, T.S. Balamurugan, S.M. Chen, T.W. Chen, Facile synthesis of orthorhombic strontium copper oxide microflowers for highly sensitive nonenzymatic detection of glucose in human blood. J. Taiwan Inst. Chem. Eng. **81**, 182–189 (2017)
24. M. Balaji, J. Chandrasekaran, M. Raja, Role of substrate temperature on MoO3 thin films by the JNS pyrolysis technique for P-N junction diode application. Mater. Sci. Semicond. Process. **43**, 104–113 (2016)
25. A.R. Ismail, R.K. Abdulnabi, O.A. Abdulrazzaq, M.F. Jawad, Preparation of MAPbI3 perovskite film by pulsed laser deposition for high-performance silicon-based heterojunction photodetector. Opt. Mater. **126**, 112147 (2022)
26. Ş Karataş, N. Berk, Performance of the illumination dependent electrical and photodiode characteristic of the Al/(GO:PTCDA)/p-Si structures. Opt. Mater. **126**, 112231 (2022)
27. R. Raj, H. Gupta, L.P. Purohit, Performance of RF sputtered V_2O_5 interface layer in p-type CdTe/Ag Schottky diode. Opt. Mater. **126**, 112176 (2022)
28. A.B. Ahmed, M. Benhaliliba, Y.S. Ocak, A. Ayeshamariam, C.E. Benouis, Photovoltaic parameters and computational spectroscopic investigation of third order nonlinear optical of CuPc/Si organic diode. Opt. Mater. **126**, 112071 (2022)
29. G. Yadav, S. Dewan, M. Tomar, Electroluminescence study of InGaN/GaN QW based pin and inverted pin junction based short-wavelength LED device using laser MBE technique. Opt. Mater. **126**, 112149 (2022)
30. S. Yang, W. Zhou, J. Qu, L. Zhang, X. Lv, Z. Zheng, X. Chen, H. Yan, M. Zhao, D. Zhuang, The impact of Ga and S concentration and gradient in Cu (In, Ga)(Se, S) 2 solar cells. Opt. Mater. **126**, 112143 (2022)
31. M. Irfan, M.I. Khan, M. Amami, R. Ahson, E.A. Alabbad, Effect of Fe ions beam on the structural, optical, photovoltaic properties of TiO2 based dye-sensitized solar cells. Opt. Mater. **123**, 111794 (2022)
32. M. Shahbazi, A. Taherkhani, Study of optical and structural properties of GO and MnO2-GO hybrid fabricated by spray pyrolysis technique. Opt. Mater. **123**, 111849 (2022)
33. C. Yadav, S. Kumar, Numerical simulation of novel designed perovskite/silicon heterojunction solar cell. Opt. Mater. **123**, 111847 (2022)
34. R. Marnadu, J. Chandrasekaran, M. Raja, M. Balaji, V. Balasubramani, Impact of Zr content on multiphase zirconium–tungsten oxide (Zr–WO_x) films and its MIS structure of Cu/Zr–WO_x/p-Si Schottky barrier diodes. J. Mater. Sci.: Mater. Electron. **29**, 2618–2627 (2018)
35. P. Harishsenthil, J. Chandrasekaran, R. Marnadu, V. Balasubramani, Incorporation of Zn ions on high dielectric HfO_2 thin films by spray pyrolysis and fabrication of Al/Zn@HfO_2/n-Si Schottky barrier diodes. Sens. Actuators A **331**, 112725 (2021)
36. P. Vivek, J. Chandrasekaran, R. Marnadu, S. Maruthamuthu, V. Balasubramani, Incorporation of Ba^{2+} ions on the properties of MoO_3 thin films and fabrication of positive photo-

response Cu/Ba–MoO_3/p-Si structured diodes. Superlattices Microstruct. **133**, 106197 (2019)
37. P. Vivek, J. Chandrasekaran, R. Marnadu, S. Maruthamuthu, V. Balasubramani, P. Balraju, Zirconia modified nanostructured MoO_3 thin films deposited by spray pyrolysis technique for Cu/MoO_3-ZrO_2/p-Si structured Schottky barrier diode application. Optik **199**, 163351 (2019)
38. R. Marnadu, J. Chandrasekaran, S. Maruthamuthu, P. Vivek, V. Balasubramani, P. Balraju, Jet nebulizer sprayed WO_3-nanoplate arrays for high-photoresponsivity based metal–insulator–semiconductor structured Schottky barrier diodes. J. Inorg. Organomet. Polym Mater. **30**, 731–748 (2020)
39. R. Marnadu, J. Chandrasekaran, P. Vivek, V. Balasubramani, S. Maruthamuthu, Impact of phase transformation in WO_3 thin films at higher temperature and its compelling interfacial role in Cu/WO_3/p–Si structured Schottky barrier diodes. Z. Phys. Chem. **234**, 355–379 (2020)
40. B. Gowtham, V. Ponnuswamy, J. Chandrasekaran, V. Balasubramani, R. Suresh, G. Pradeesh, S. Ramanathan, Effect of surface modification of WO3 nanostructures on the performance for p-Si/n-WO_3 structure diodes. Inorg. Chem. Commun. **130**, 108695 (2021)
41. B. Gowtham, V. Balasubramani, S. Ramanathan, M. Ubaidullah, S.F. Shaikh, G. Sreedevi, Dielectric relaxation, electrical conductivity measurements, electric modulus and impedance analysis of WO_3 nanostructures. J. Alloy Compd. **888**, 161490 (2021)
42. P. Harishsenthil, J. Chandrasekaran, D. Thangaraju, V. Balasubramani, Fabrication of strontium included hafnium oxide thin film-based Al/Sr: HfO_2/n-Si MIS-Schottky barrier diodes for tuned electrical behavior. New J. Chem. **45**, 19476–19486 (2021)
43. S. Altındal, A. Barkhordari, S. Özçelik, G. Pirgholi-Givi, H.R. Mashayekhi, Y. Azizian-Kalandaragh, A comparison of electrical characteristics of Au/n-Si (MS) structures with PVC and (PVC: Sm_2O_3) polymer interlayer. Phys. Scr. **96**, 125838 (2021)
44. J. Farazin, M.S. Asl, G. Pirgholi-Givi, S.A. Delbari, A.S. Namini, Ş Altındal, Y. Azizian-Kalandaragh, Effect of (Co–TeO2-doped polyvinylpyrrolidone) organic interlayer on the electrophysical characteristics of Al/p-Si (MS) structures. J. Mater. Sci.: Mater. Electron. **32**(17), 21909–21922 (2021)
45. E. Yükseltürk, O. Surucu, M. Terlemezoglu, M. Parlak, S. Altındal, Illumination and voltage effects on the forward and reverse bias current–voltage (IV) characteristics in In/In_2S_3/p-Si photodiodes. J. Mater. Sci.: Mater. Electron. **32**, 21825–21836 (2021)
46. A. Kaymaz, E. Evcin Baydilli, H. Uslu Tecimer, Ş Altındal, Y. Azizian-Kalandaragh, Evaluation of gamma-irradiation effects on the electrical properties of Al/(ZnO-PVA)/p-Si type Schottky diodes using current-voltage measurements. Radiat. Phys. Chem. **183**, 109430 (2021)
47. A. Tataroğlu, S. Altındal, Y. Azizian-Kalandaragh, Electrical characterization of Au/n-Si (MS) diode with and without graphene-polyvinylpyrrolidone (Gr-PVP) interface layer. J. Mater. Sci.: Mater. Electron. **32**, 3451–3459 (2021)
48. S. Demirezen, H.G. Çetinkaya, M. Kara, F. Yakuphanoğlu, S. Altındal, Synthesis, electrical and photo-sensing characteristics of the Al/(PCBM/NiO:ZnO)/p-Si nanocomposite structures. Sens. Actuators A **317**, 112449 (2021)
49. Ç.Ş Güçlü, A.F. Özdemir, A. Karabulut, A. Kökce, S. Altındal, Investigation of temperature dependent negative capacitance in the forward bias CV characteristics of (Au/Ti)/Al_2O_3/n-GaAsSchottky barrier diodes (SBDs). Mater. Sci. Semicond. Process. **89**, 26–31 (2019)
50. Y. Şafak-Asar, T. Asar, S. Altındal, S. Özçelik, Investigation of dielectric relaxation and ac electrical conductivity using impedance spectroscopy method in (AuZn)/TiO_2/p-GaAs (1 1 0) Schottky barrier diodes. J. Alloy. Compd. **628**, 442–449 (2015)
51. A. Sahar, S. Altındal, E.E. Tanrıkulu, D.E. Yıldız, Analysis of temperature dependent current-conduction mechanisms in Au/TiO_2/n-4H-SiC (metal/insulator/semiconductor) type Schottky barrier diodes. J. Appl. Phys. **116**, 083709 (2014)
52. E.E. Tanrıkulu, S. Demirezen, Ş Altındal, İ Uslu, Analysis of electrical characteristics and conduction mechanisms in the Al/(%7 Zn-doped PVA)/p-Si (MPS) structure at room temperature. J. Mater. Sci.: Mater. Electron. **28**, 8844–8856 (2017)
53. A. Eroğlu, S. Demirezen, Y. Azizian-Kalandaragh, S. Altındal, A comparative study on the electrical properties and conduction mechanisms of Au/n-Si Schottky diodes with/without an organic interlayer. J. Mater. Sci.: Mater. Electron. **31**, 14466–14477 (2020)
54. S. Altındal, A. Barkhordari, G. Pirgholi-Givi, M. Ulusoy, H.R. Mashayekhi, S. Özçelik, Y. Azizian-Kalandaragh, Comparison of the electrical and impedance properties of Au/(ZnOMn:PVP)/n-Si (MPS) type Schottky-diodes (SDs) before and after gamma-irradiation. Phys. Scr. **96**, 125881 (2021)
55. M. Ulusoy, S. Altındal, Y. Azizian-Kalandaragh, S. Özçelik, Z. Mirzaei-Kalar, The electrical characteristic of an MIS structure with biocompatible minerals doped (Brushite+Monetite: PVC) interface layer. Microelectron. Eng. **258**, 111768 (2022)
56. A.A. Alsaç, T. Serin, S.O. Tan, S. Altındal, Identification of current transport mechanisms and temperature sensing qualifications for Al/(ZnS-PVA)/p-Si structures at low and moderate temperatures. IEEE Sens. J. **22**, 99–106 (2022)

57. S.O. Tan, İ Taşcıoğlu, S. Altındal Yerişkin, H.Ü.S.E.Y.İN. Tecimer, F. Yakuphanoğlu, Illumination dependent electrical data identification of the cdzno interlayered metal-semiconductor structures. Silicon **12**, 2885–2891 (2020)
58. Ö. Vural, Y. Şafak, S. Altındal, A. Türüt, Current–voltage characteristics of Al/Rhodamine-101/n-GaAs structures in the wide temperature range. Curr. Appl. Phys. **10**, 761–765 (2010)
59. H. Altuntaş, S. Altındal, H. Shtrikman, S. Özçelik, A detailed study of current–voltage characteristics in Au/SiO2/n-GaAs in wide temperature range. Microelectron. Reliab. **49**, 904–911 (2009)
60. M. Moeen, M. Kolahdouz, A. Salemi, A. Abedin, M. Östling, H.H. Radamson, Improved designs of Si-based quantum wells and Schottky diodes for IR detection. Thin Solid Films **613**, 19–23 (2016)
61. M. Sakthivel, S.S. Mary, V. Balasubramani, A. Ibrahim, J. Hakami, V.R. Reddy, The optical and electrical properties of Ba thin films for junction diode application by jet nebulizer spray pyrolysis method. Inorg. Chem. Commun. **141**, 109511 (2022)
62. H. Aydin, A. Tataroğlu, A.A. Al-Ghamdi, F. Yakuphanoglu, F. El-Tantawy, W.A. Farooq, A novel type heterojunction photodiodes formed junctions of Au/LiZnSnO and LiZnSnO/p-Si in series. J. Alloys Compds. **625**, 18–25 (2015)
63. A. Tataroğlu, Ş. Altındal, M. M. Bülbül. 60Co γ irradiation effects on the current–voltage (I–V) characteristics of Al/SiO2/p-Si (MIS) Schottky diodes. Nucl. Instrum. Methods Phys. Res. A. **568**(2), 863-868 (2006)